Article

Synthesis of Green Brucite [Ni$_x$Mg$_{1-x}$(OH)$_2$] by Incorporation of Nickel Ions in the Periclase Phase (MgO) Applied as Pigments

Cássio Siqueira [1], Aline B. Schons [1], Patricia Appelt [1], Weslei D. Silva [2], Nayara Balaba [1], Mário A. A. Cunha [2] and Fauze J. Anaissi [1,*]

[1] Department of Chemistry, Universidade Estadual do Centro-Oeste, UNICENTRO, Alameda Elio Antonio Dalla Vecchia, 838, Guarapuava 85040-167, PR, Brazil; cassiosiqueira19@gmail.com (C.S.); patriciaappelt@unicentro.br (P.A.); nayarabalaba20@gmail.com (N.B.)

[2] Department of Chemistry, Universidade Tecnológica Federal do Paraná, UTFPR, Via do Conhecimento, KM 01, Pato Branco 85503-390, PR, Brazil; wesleisilva@alunos.utfpr.edu.br (W.D.S.); mcunha@utfpr.edu.br (M.A.A.C.)

* Correspondence: anaissi@unicentro.br

Abstract: Magnesium oxide is typically white and can be colorized with transition metal insertion by doping. We present the preparation of a green-colored hydroxide by the exchange of Mg^{2+} on the crystalline lattice with Ni^{2+} in MgO, using three nickel salts. MgO$_{st}$ was prepared by the colloidal starch suspension method, using cassava starch. The oxides and hydroxides, before and after, were characterized by X-ray diffraction (XRD), and show that a phase change occurs: a transition from periclase (MgO) to brucite (Mg(OH)$_2$) due to the incorporation of nickel ions from different salts (acetate, chloride, and nitrate), resulting in the solid solution [Ni$_x$Mg$_{1-x}$(OH)$_2$]. The FTIR spectrum corroborates the crystallographic structure identified through XRD patterns, confirming the formation of a crystal structure resembling brucite. The new samples present a green color, indicative of the incorporation of the Ni^{2+} ions. The antimicrobial activity of products resulting from the doping of magnesium oxide with nickel and the precursor MgO$_{st}$ was assessed through the minimum inhibitory concentration (MIC) test. The evaluation included three bacterial strains: *Staphylococcus aureus* (ATCC 25923), *Escherichia coli* (ATCC 25922), *Salmonella gallinarum* (ATCC 9184), and a yeast strain, *Candida albicans* (ATCC 10231). The obtained results were promising; the tested samples exhibited antimicrobial activity, with a MIC ranging from 0.312 to 0.625 µg·µL^{-1}. The nickel compound, derived from the precursor chloride salt, demonstrated superior MIC activity. Notably, all tested samples displayed bactericidal activity against the *S. aureus* strain and exhibited a broad spectrum of inhibition, encompassing both Gram-positive and Gram-negative strains. Only the nickel compounds derived from precursors with acetate and nitrate anions demonstrated antimicrobial activity against *C. albicans*, exhibiting a fungistatic behavior. Based on the conducted studies, [Ni$_x$Mg$_{1-x}$(OH)$_2$] has emerged as a promising antimicrobial agent, suitable for applications requiring the delay or inhibition of bacterial growth.

Keywords: solid solution; magnesium oxide; inorganic pigment; antimicrobial activity

1. Introduction

Recently, the compound MgO has attracted attention due to its properties, including diverse nanostructures, a high surface area, and nontoxicity [1]. As a result, various fields are exploring applications such as catalysis [2], superconductor [3], biological activities [4–6], treatment of wastewater [7], and pigments [1]. The usual route to obtain MgO is through Mg(OH)$_2$ calcination [8]. According to previous works, MgO and Mg(OH)$_2$ are interchangeable, depending on the procedure of hydration or dehydration [9]. The use of organic fuel for the synthesis of MgO has been shown to be advantageous due to its low cost, lowering of the calcination temperature, and eco-friendly behavior [4].

Particularly, water treatment studies have demonstrated MgO's efficiency in the removal of Ni^{2+} and Cu^{2+}, as well as other metal ions, through precipitation in the stable compound of the brucite crystal phase ($Mg(OH)_2$) [10,11]. Hence, discovering new applications for the precipitate originating from water treatment with MgO may be of interest from the ecological standpoint, as it involves repurposing a byproduct of an already beneficial process. These solid solutions of hydroxides have only been reported to be employed as supercapacitors [3,12,13].

Furthermore, metal oxides and hydroxides serve as common hosts for transition metal chromophores in the inorganic pigments field [14–16]. The variation of the supporting structure or transition metal chromophores constitutes a methodology to enhance known inorganic pigments or synthesize novel ones, envisioning the implication on economics, efficiency, and ecological aspects [14].

Moreover, nickel is commonly implemented in support structures as chromophores in inorganic pigments, often associated with yellow, blue, and green colors [17–19]. Additionally, MgO also exhibits biological activity properties as an antimicrobial, antioxidant, and antifungal [20,21] agent. Moreover, nickel oxide also presents antimicrobial activity [22,23].

Hence, the present work describes a fast and easy route to synthesize $[Ni_xMg_{1-x}(OH)_2]$ and its potential application as an inorganic pigment with antimicrobial features. To the best of our knowledge, no prior use of $[Ni_xMg_{1-x}(OH)_2]$ for this purpose has been reported in the literature. Therefore, the objective of the paper is to synthesize $[Ni_xMg_{1-x}(OH)_2]$ green-colored pigments and characterize these compounds by evaluating the influence of the precursor salt anion. In addition, the minimum inhibitory concentration (MIC) biological test was carried out to check the inhibition activity of the product in solution against Gram-positive and Gram-negative bacteria and yeast. The aim of this test is, in future work, to verify the biological inhibition effectiveness of the paint pigmented with $[Ni_xMg_{1-x}(OH)_2]$. The strains tested were the yeast *Candida albicans*, and the bacteria *Staphylococcus aureus*, *Escherichia coli*, and *Salmonella gallinarum*, which are disease-causing microorganisms and cause concern for public health, as cited by the World Health Organization [24–26]. With this in mind, and verifying the possibility of the paint pigmented with the compound $[Ni_xMg_{1-x}(OH)_2]$ maintaining its antimicrobial properties, its use is considered for application in indoor and outdoor environments with a high probability of microorganism proliferation [27].

2. Materials and Methods

2.1. Synthesis of MgO from Cassava Starch

The utilized MgO was synthesized by the same route as Balaba et al. [4], using cassava starch. The experimental procedure began with the extraction of starch (500 g) in 2.5 L of deionized water under stirring for 3 h followed by sieving. Then the synthesized starch (300 g) was added to a beaker together with magnesium nitrate (64 g) and left to react for 20 min under agitation. This mixture was calcinated at 750 °C for 1 h with a heating ramp of 10 °C min^{-1}. The white solid was pulverized using a pestle and mortar and identified as MgO_{st}.

2.2. Synthesis of [Ni_xMg_{1−x}(OH)_2] Pigments

The pigments were produced by combining the MgO_{st} and nickel salts, with the salts being nickel acetate tetrahydrate [$Ni(C_2H_3O_2)_2.4H_2O$], P.A., Neon], nickel chloride hexahydrate [$Ni(Cl)_2.6H_2O$), P.A., Neon], and nickel nitrate hexahydrate [$Ni(NO_3)_2.6H_2O$), P.A., Neon]. The reaction was conducted in a medium of 60 mL of deionized water, where MgO_{st} (1 g) and the respective nickel salt (10 mL, 0.5 M, stock solution) were blended and stirred by the magnetic bar for 30 min. Subsequently, the precipitate was separated from the medium by centrifugation, washed with deionized water, and left to dry in a desiccator. Finally, the powder was sieved through a 250-mesh sieve. The samples were named Ni(Ac) for the acetate, Ni(Chlo) for chloride, and Ni(Nitr) for nitrate, only to differentiate the product obtained from salts with different anions.

2.3. Dispersion of Pigments in Paint

The application as synthetic inorganic pigments was made by dispersing 10% by mass of the powders in a commercial colorless paint in a 2:1 paint/water proportion. The pigmented paint was applied in two coats (the second after natural drying) on gypsum blocks.

2.4. Characterization of Compounds

The elemental composition of the structured MgO_{st} and after adsorption of nickel were evaluated using an energy-dispersive X-ray spectrometer (EDXRF) (Shimadzu, Kyoto, Japan), model EDX-7000, containing an Rh tube, operating at 50 and 15 W. The crystalline structure and phase were characterized by X-ray diffractometry (XRD-D2 Phaser; Bruker, Billerica, MA, USA), with a copper cathode (λ = 1.5418 Å), 30 kV potential, 10 mA current, ranging between 10° and 80° (2θ), and with 0.2°/s increments. The crystallographic charts used were from the International Centre of Diffraction Data (ICDD, Newtown Square, PA, USA). Furthermore, the crystallinity was determined by the software Difracc.EVA (version 3.0) utilizing the 100% peak. The morphology of the MgO_{st} particulate and the samples containing nickel were examined with a scanning electron microscope (SEM—Tescan Vega3, Kohoutovice, Czech Republic) with an accelerating voltage of 20 kV. Fourier transform infrared spectroscopy was performed in a Perkin Elmer Frontier device (Waltham, MA, USA). The samples were analyzed in the attenuated total reflectance (ATR) mode. The colorimetric analysis was performed on the MgO_{st} and the green pigments in the powder form, and after application in the colorless paint, with a portable colorimeter (3 nh, model NR60CP, Guangzhou, China) with a D65 light source. The optical diffuse reflectance and absorbance were measured on the pigments in powder form and dispersed in colorless paints (UV-VIS-NIR Spectrophotometer CARYb5G, Varian, Palo Alto, CA, USA) in the range of 400–900 nm. The painted plaster blocks were characterized with the same spectrophotometer and colorimeter mentioned previously. The data representative of colorimetric (CIE L*a*b*) analyses are as follows: The L* parameter is the brightness and ranges from 0 to 100. The parameter a* represents the variation between red and green, where +a tends to red and −a* tends to green. The parameter b* is the variation between blue and yellow, where +b* tends to yellow and −b* tends to blue. The h* parameter refers to the hue angle (tan − 1 b*/a*). The value of C* is the chroma and represents the color saturation of the samples [28].

2.5. Microbiological Testing

2.5.1. Minimal Inhibitory Concentration (MIC) Determination

The minimum inhibitory concentration (MIC) determination assay was conducted to assess the spectrum of action of the samples based on the resistance of the studied microorganisms. The tested microorganisms were acquired from the American Type Culture Collection (ATCC). The test was performed according to the Clinical and Laboratory Standards Institute (CLSI) standards [29,30]. The antimicrobial potential of both the precursor salt, magnesium oxide, and the products derived from syntheses (nickel-doped magnesium oxide with three different anions: acetate, chloride, and nitrate) was evaluated. The strains tested were the yeast *Candida albicans* (ATCC 10231), the Gram-positive bacterium *Staphylococcus aureus* (ATCC 25923), and the Gram-negative bacteria *Escherichia coli* (ATCC 25922) and *Salmonella gallinarum* (ATCC 9184).

The stock cultures were preserved on slants of Brain Heart Infusion (BHI) Agar for bacteria or Sabouraud dextrose agar (SDA) for yeast in tubes covered with sterile mineral oil and maintained at 4 °C. Activation of the cultures involved transferring a loopful of cells to tubes containing Mueller Hinton agar (for bacteria) or Sabouraud dextrose agar (for yeast), followed by cultivation at 37 °C for 24 h (for bacteria) or at 28 °C for 48 h (for yeast). Microbial inoculum was obtained by suspending active cultures in saline solution at a concentration of 1.5×10^8 CFU mL^{-1} (0.5 McFarland scale: absorbency of 0.08–0.13 at 625 nm). Standard solutions of the tested compounds were prepared at a ratio of 1.25 µg µL^{-1} (*w/v*) in 10% dimethyl sulfoxide (DMSO: previously tested non-cytotoxic

concentration). Microdilutions were performed in 96-well plates using serial dilutions of the antimicrobial compounds. The compounds were examined at concentrations ranging from 0.625 to 0.0048 µg µL^{-1}. A volume of 100 µL of specific culture medium for each microorganism (bacteria, Mueller Hinton broth; yeast, Sabouraud broth), 100 µL of different concentrations of the tested compound, and 20 µL of the microbial suspension was added to the wells. The plates were incubated for 24 h at 37 °C (bacteria) or 48 h at 28 °C (yeast). The experiment employed chloramphenicol (1.2 mg/mL for bacteria) and fluconazole (100 mg/mL for yeast) as positive controls. Conversely, the negative controls comprised a 10% (*v/v*) solution of dimethyl sulfoxide (DMSO) as the solvent control, and the growth control, which exclusively involved the culture medium.

After the incubation, a 2,3,5-triphenyl-tetrazolium chloride (TTC) solution (0.125% *w/v*, 20 µL) was added to all wells, and the plates were incubated again for another two hours. The minimum inhibitory concentration (MIC) was read for each microorganism and compound tested by observing the color present in each well of the plate. The appearance of a pink color indicated the presence of viable cells, while the unchanged color of the medium indicated a positive result for microbial inhibition.

2.5.2. Minimal Bactericidal or Fungicidal Concentration (MBC/MFC) Determination

The determination of the minimum bactericidal concentration (MBC) or minimum fungicidal concentration (MFC) was performed after the MIC reading, following the procedure recommended by the Clinical and Laboratory Standards Institute (CLSI) [29,30]. Subsequently, wells exhibiting inhibitory effects in the MIC test were transferred to Petri plates containing the respective culture medium (Mueller Hinton agar for bacteria; Sabouraud dextrose agar for yeasts). The plates were then incubated for the specific duration required for each microorganism. Following incubation, the presence or absence of colony growth was examined, facilitating the characterization of the compound as either bacteriostatic/fungistatic or bactericidal/fungicidal.

3. Results

3.1. Characterization of Periclase and Green Brucite

3.1.1. Chemical Analysis of Samples by EDXRF

The composition of the samples, concerning the percentage of nickel, was estimated by chemical analysis by energy dispersive X-ray fluorescence (EDXRF), and the results are in Table 1.

Table 1. EDXRF element analysis.

Nickel Precursor Salt	Mg (%)	Ni (%)	Estimated Composition
MgO$_{st}$	99.841	-	[Mg$_{0.99}$O]
Acetate	90.867	8.789	[Ni$_{0.087}$Mg$_{0.91}$(OH)$_2$]$_{Ac}$
Chloride	90.784	9.050	[Ni$_{0.090}$Mg$_{0.91}$(OH)$_2$]$_{Chlo}$
Nitrate	90.342	9.437	[Ni$_{0.094}$Mg$_{0.90}$(OH)$_2$]$_{Nitr}$

The results point to a gradual increase in the number of nickel ions incorporated by MgO$_{st}$, this fact being associated with the solubility of the precursor salts. According to Haynes et al. [31], nickel(II) nitrate hexahydrate has a solubility of 99.2 g/100 mL H$_2$O (number #1886), is more soluble than nickel(II) chloride hexahydrate that presents a solubility of 67.5 g/100 mL H$_2$O (#1874), and the latter is more soluble than nickel(II) acetate tetrahydrate that has a solubility of 16 g/100 mL H$_2$O (#1864).

The interaction of the periclase phase with Ni^{2+} ions result in the formation of the brucite phase (Equation (1)), whose estimated composition is presented in Table 1.

$$\text{MgO (periclase phase)} + \text{Ni}^{2+}_{(aq)} \rightarrow \text{Ni}_x\text{Mg}_{1-x}(\text{OH})_2 \text{ (brucite phase)} \tag{1}$$

3.1.2. Structural Analysis by X-ray Diffraction (XRD)

The X-ray diffraction profile of the MgO$_{st}$ sample (Figure 1) identifies the MgO periclase phase (ICDD: 01-075-0447), characterized by a face-centered cubic structure, with characteristic peaks (111), (200), (220), (311), and (222) [32,33].
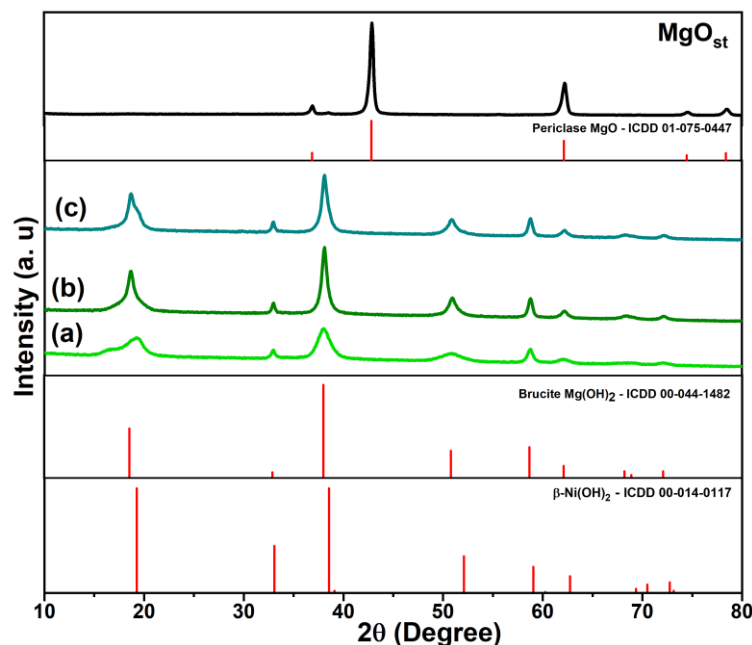

Figure 1. XRD profile of periclase (MgO$_{st}$) and green brucite [Ni$_x$Mg$_{1-x}$(OH)$_2$], with samples being (a) Ni(Ac), (b) Ni(Nitr), and (c) Ni(Chlo). The figure includes the XRD patterns of the periclase and brucite phases from the ICDD database.

As shown in the X-ray diffraction profile (Figure 1) of the [Ni$_x$Mg$_{1-x}$(OH)$_2$] samples, the characteristic peaks identified were (001), (100), (101), (102), (110), (111), (103), (200), and (201), being this crystalline phase determined as brucite, a hexagonal arrangement of Mg(OH)$_2$ (ICDD: 00-044-1482) [3,33,34]. Moreover, β-Ni(OH)$_2$ is isostructural to Mg(OH)$_2$ with a brucite-like crystal lattice [3,35].

3.1.3. Morphological Behavior by Scanning Electronic Microscopy (SEM)

SEM images of the samples are shown in Figure 2. The MgO$_{st}$ subjected to the same process of hydration without the presence of nickel ion in solution exhibits a plate-like morphology (Figure 2a), already reported in the literature for Mg(OH)$_2$, which corresponds to the brucite lamellar structure [36,37]. The green pigments show the same plate-like morphology, as depicted in Figure 2b–d. The Ni(Chlo) sample (Figure 2c) presented a needle shape which can be attributed to the Cl$^-$ ion in the reaction medium [38] in addition to the plate morphologies that form the agglomerates.
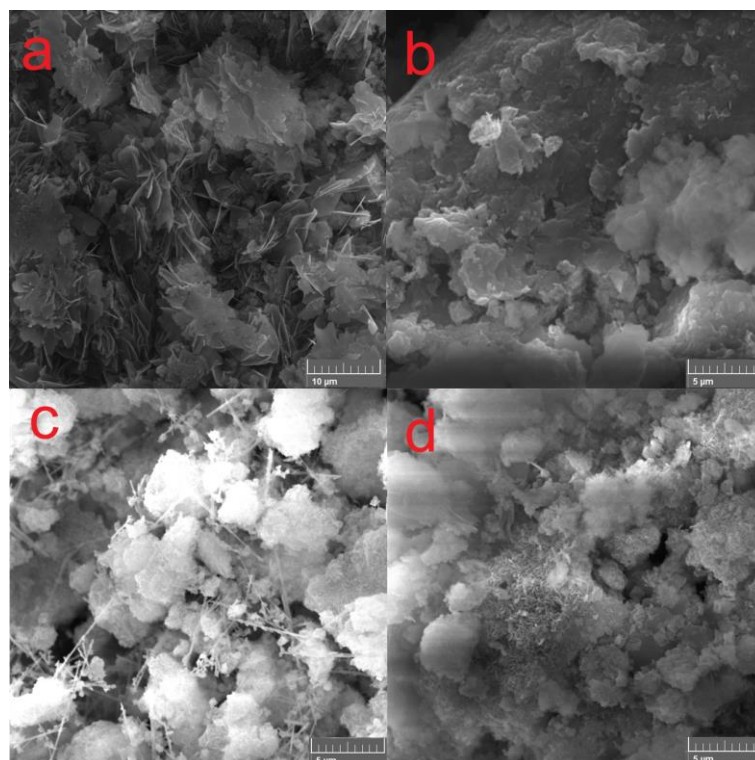
Figure 2. SEM images of compounds (**a**) MgO$_{st}$, (**b**) Ni(Ac), (**c**) Ni(Chlo), and (**d**) Ni(Nitr).

3.1.4. Fourier Transform Infrared Spectroscopy (FTIR)

The FTIR vibrational spectra show specific differences between the samples depending on the residual functional groups of the nickel salts used to prepare the green pigments. The infrared spectrum (Figure 3) identified the stretching of hydroxyl ν(OH) at 3691 cm^{-1} for all compounds and the wide band at 3358 cm^{-1} for the samples with Ni^{2+} [33,35].
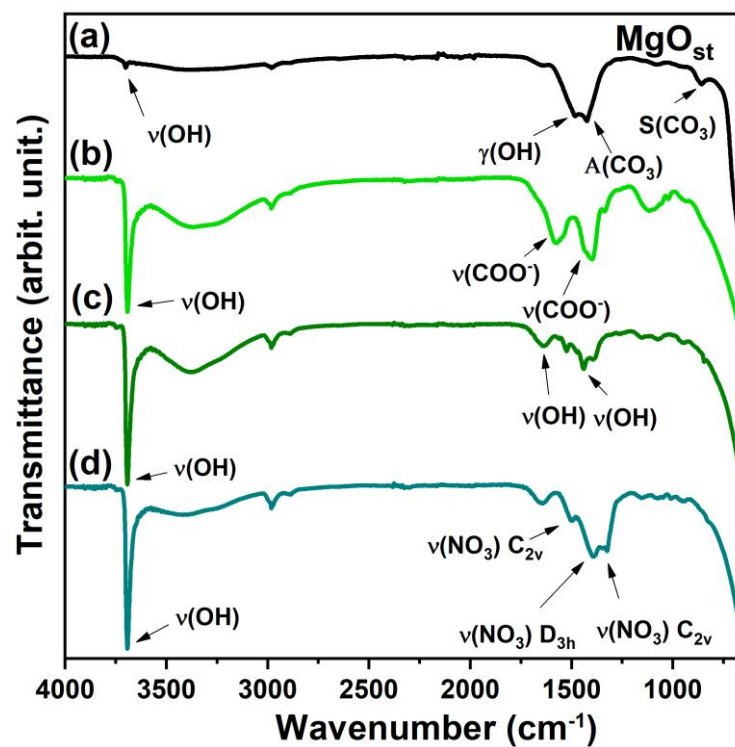
Figure 3. FTIR spectrum. (**a**) MgO$_{st}$; (**b**) Ni(Ac); (**c**) Ni(Chlo); (**d**) Ni(Nitr).

The $\gamma(OH)$ region of the MgO_{st} sample (Figure 3a) exhibits a band at 1486 cm^{-1}, which corresponds to the O-H bending mode. This mode is characterized by the bending vibration of the -OH group of the physisorbed water molecules [4].

The bands at 1425 and 1085 cm^{-1} were attributed to the asymmetric and symmetric stretching of an unidentate carbonate on the surface, respectively [4,39]. The bands in the spectrum after the incorporation of Ni^{2+} (Figure 3b) at 1582 and 1398 cm^{-1} are from the symmetrical and asymmetrical $\nu(COO^-)$ [40,41].

The bands around 1652 and 1443 cm^{-1} for the sample synthesized by chloride (Figure 3c) correspond to the $\nu(OH)$ of the water molecule physisorbed in the lattice [4,33]. For the compound synthesized by nitrate, the band of vibration modes of $\nu(NO_3)$ inter-layered are shown in the spectrum (Figure 3d) at 1384 cm^{-1}, and the other two bands at 1509 and 1323 cm^{-1} are associated with metal coordinated nitrate [41].

3.1.5. Colorimetric Analysis and Visible-NIR Spectroscopy

The absorption spectrum in the visible region (Figure 4a) shows characteristic bands for solid samples of green pigments $[Ni_xMg_{1-x}(OH)_2]$ at 678 nm and 745 nm. Complementarily, the diffuse reflectance spectra (Figure 4b) show bands with reflectance maxima in the visible region (450–600 nm), and above the near-infrared region (800 nm).

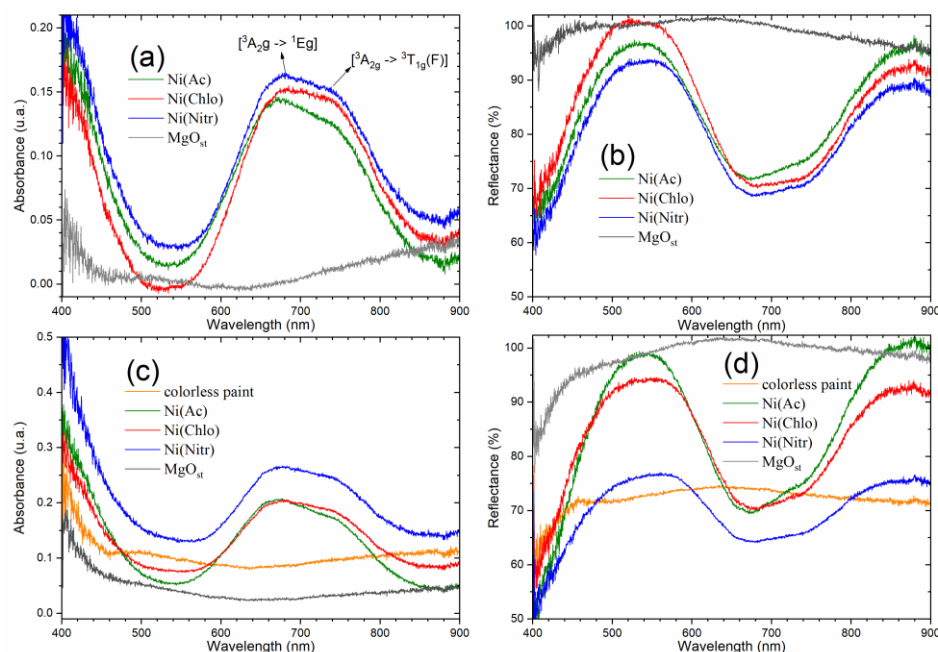**Figure 4.** Electronic spectrum of absorbance and reflectance of solids. (**a**,**b**) powder pigments; (**c**,**d**) dispersed on colorless paint.

The bands are attributed to the Laporte transitions of the ground state $[^3A_{2g} \rightarrow ^1E_g]$ and $[^3A_{2g} \rightarrow ^3T_{1g}(F)]$ of nickel [42–44].

The absorption spectra of pigments dispersed in paint (Figure 4c,d) show the same band profile characteristic of powder pigments, due to good dispersion and the chemical stability of the pigments, that is, they do not react with the paint. The behavior of the pigment of nitrate as a precursor conveys more absorbance on the paint and consequently less reflectance. On the contrary, acetate and chloride increase the paint reflectance, due to acetate being more reflective in paint.

The colorimetric analysis utilizing CIE L*a*b* color space is displayed in Table 2 for the powdered pigments. From the data, it was observed that despite the different precursor salts, the samples did not show significant discrepancies between the CIE L*a*b* values. All the samples maintained the values in the quadrants green ($-a^*$) and yellow ($+b^*$). Similarly, there was no significant difference between the ΔE color difference values, which were ~17.

Table 2. Colorimetric analysis of pigments in powder form.

Sample	L*	a*	b*	C*	h*	ΔE	Color Mine
MgO$_{st}$	67.65	0.84	3.13	3.24	104.98	-	
Ni(Ac)	54.02	−8.56	7.61	11.45	138.34	17.15	
Ni(Chlo)	54.28	−9.39	6.46	11.40	145.48	17.16	
Ni(Nitr)	54.35	−9.03	6.96	11.40	142.37	17.00	

The pigments were dispersed in colorless paint and applied to paper. The test specimens were also evaluated according to the CIE L*a*b* metrics (Table 3) and were also applied to plaster blocks (Table 4) for comparison purposes. After the dispersion, the L* values increased due to the interference of the color of the paper and plaster. For the pigments on paper, the discrepancy color was observed for the chloride pigment Ni(Chlo), where the ΔE showed a lower value compared to the colorless paint. For the samples dispersed in colorless paint and applied to the blocks, the lowest color variation was for the nitrate pigment with a value of ~8.5.

Table 3. Colorimetric analysis of colorless paint pigments dispersed on paper.

Sample	L*	a*	b*	C*	h*	ΔE	Color Mine
Colorless paint	65.04	−0.95	2.91	3.06	108.14	-	
MgO$_{st}$	78.49	0.54	4.42	4.45	96.90	13.62	
Ni(Ac)	70.60	−13.07	10.67	16.87	140.77	15.43	
Ni(Chlo)	64.59	−9.20	7.64	11.96	140.31	9.52	
Ni(Nitr)	72.36	−12.22	11.13	16.53	137.68	15.75	

Table 4. Colorimetric analysis of colorless paint pigments dispersed on plaster block.
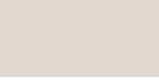
Sample	L*	a*	b*	C*	h*	ΔE	Color Mine
Colorless paint	88.00	−0.06	4.37	4.37	90.34	-	
MgO$_{st}$	86.99	0.53	4.42	4.45	96.90	1.17	
Ni(Ac)	82.87	−7.48	10.65	13.01	125.07	11.00	
Ni(Chlo)	83.46	−6.77	9.07	11.31	126.75	9.37	
Ni(Nitr)	85.49	−5.83	10.03	11.60	120.16	8.46	

Figure 5 shows the comparative difference in color of the green pigments and the white pigment (MgO$_{st}$). It is clear that inorganic nickel salts (acetate, chloride, and nitrate) do not affect luminosity, L*, values, which are very close. There is a small difference in the a* and b* values, which indicate that they are in the yellow-green quadrant (a negative, b positive), reflecting the behavior of a green-yellow pigment, due to the presence of the Ni^{2+} ion.

(a) **(b)** **(c)**

Ni^{2+}

MgO$_{St}$ Ni(Ac) Ni(Chlo) Ni(Nitr)

L* 67.65 | L* 54.35 | L* 54.28 | L* 54.02
a* 0.84 | a* −9.03 | a* −9.39 | a* −8.56
b* 3.13 | b* 6.96 | b* 6.46 | b* 7.61
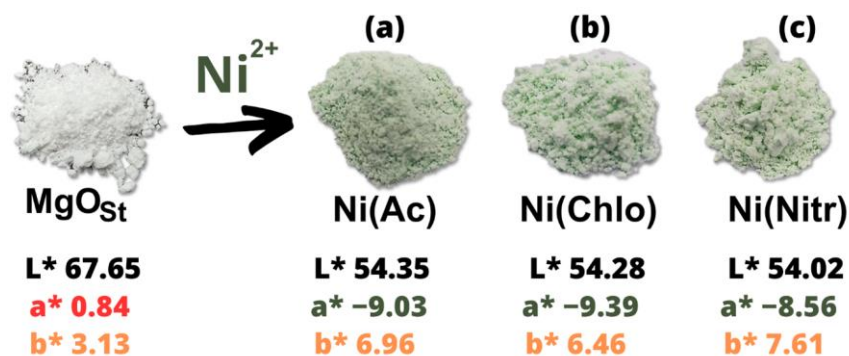
Figure 5. CIE L*a*b* parameters powder pigment, after and before adsorption of nickel with the salt of (**a**) Ni(Ac), (**b**) Ni(Chlo), and (**c**) Ni(Nitr).

3.2. Microbiological Tests (MIC, MBC and MFC)

In general, the microbiological tests showed good results for the compounds; all oxides presented antimicrobial activity at the examined concentrations. These findings suggest that the tested compounds can serve as effective antimicrobial agents.

An identical MIC value (0.625 µg/µL) was observed for the Gram-positive strain of *Staphylococcus aureus* and the Gram-negative strain of *Salmonella gallinarum*. This uniformity in results suggests a potentially broad spectrum of activity, indicating efficacy against bacterial strains.

In the case of *Escherichia coli*, consistent results were observed among the compounds MgO$_{st}$, Ni(Ac), and Ni(Nitr), each demonstrating a MIC of 0.625 µg/µL. Notably, the Ni(Chlo) sample exhibited enhanced activity, with a lower minimum inhibitory concentration of 0.312 µg/µL. This heightened efficacy can be attributed to the variance in the chloride anion within the compound's structure, as previously discussed in the literature [45,46].

In the MBC assay targeting *S. aureus*, all compounds demonstrated bactericidal potential at 0.625 µg/µL. Conversely, in the case of *E. coli*, all compounds exhibited bacteriostatic

effects at the same concentration, except for Ni(Chlo), which displayed bacteriostatic action at a lower concentration (0.312 μg/μL). Regarding *S. gallinarum*, the compounds restrained growth at 0.625 μg/μL, exhibiting bacteriostatic properties. However, Ni(Nitr) distinguished itself by manifesting a bactericidal effect at the specified concentration.

For the yeast *Candida albicans*, only the compounds with acetate counter-ions, Ni(Ac), and nitrate, Ni(Nitr), promoted growth inhibition of the microorganisms at a concentration of 0.625 μg/μL. However, colonies were observed after incubation in the MFC assay, classifying them as fungistatic compounds.

Notably, the compounds demonstrated superior activity against bacteria compared to the tested fungus. The bactericidal effect of all four compounds against the *S. aureus* strain is particularly noteworthy, showcasing more significant inhibition against the Gram-positive strain. Among the studied compounds, Ni(Nitr) stands out for its activity against all four microorganisms. It exhibited biocidal action against Gram-positive *S. aureus* and Gram-negative *S. gallinarum*, biostatic action on *E. coli*, and fungistatic action against the yeast *C. albicans*, highlighting its superior inhibition potential among the four compounds tested.

4. Discussion

This study presents a simple route for the synthesis of green pigments from nickel salts and magnesium oxide based on solution–base hydroxide formation. As presented by the XRD, Figure 1, the structural crystalline phase identified was the $Mg(OH)_2$ brucite. Furthermore, $β$-$Ni(OH)_2$ is isostructural to $Mg(OH)_2$ [4,35]. In this case, to distinguish the compounds from a simple mixture of $Mg(OH)_2$ and $β$-$Ni(OH)_2$, the FTIR spectra (Figure 3) indicate that the compounds form a solid solution of $[Ni_xMg_{1-x}(OH)_2]$. This is evidenced by the band at 3691 cm^{-1}, which corresponds to the metal-O covalency interaction. Compared to $β$-$Ni(OH)_2$, the O-H bond becomes less polarized with a higher concentration of Mg in the lattice, shifting the $ν(OH)$ band to higher wavenumbers [35]. Therefore, the difference in electronegativity of Mg [14,16] and Ni [6,16] promotes the exchange of Mg for Ni in the crystalline structure [35].

The influence of the precursor salts on $[Ni_xMg_{1-x}(OH)_2]$ was analyzed. The acetate anion influenced the crystalline lattice, producing a more amorphous compound [34], showing a calculated crystallinity of 85% when compared to the precursor phase periclase MgO_{st}, with 95%. As is reported in the literature for $β$-$Ni(OH)_2$, and displayed on the diffractogram Figure 2a, this disordering of the crystalline lattice is attributed to intercalation of the anion (CH_3COO^-) in the hexagonal structure [3,34]. Relating to the XRD data, Figure 5b, the FTIR bands at 1568 cm^{-1} and 1391 cm^{-1} identify the $ν(COO^-)$ symmetric and asymmetric vibration modes [40,41], reinforcing the evidence of intercalation of the acetate anion on the structure. The compounds Ni(Nitr) and Ni(Chlo) demonstrated the same crystallinity of 88%. Moreover, the splitting of peak (*001*) in the Ni(Ac) and Ni(Chlo) compounds is characteristic of the interstratification disorder of $Ni(OH)_2$, by forming layers of $α$-$Ni(OH)_2$ and $β$-$Ni(OH)_2$, and the broadening or splitting of the reflective plane is related with the loss of order along the c-axis [47,48].

The SEM analysis (Figure 2) of the $[Ni_xMg_{1-x}(OH)_2]$ compounds reveals plate-like morphologies. However, the precursor salt anion slightly affects the morphological aspects. It is worth noting that for the Ni(Chlo) precursor compound, the lamellar plate-like morphology was accompanied by needle-shaped morphologies highlighted in Figure 2c, which can correlate to the formation of a 1D-like structure from the hexagonal configuration [7,38]. Hao et al. [38] explain that the mechanism for the formation of nanotubes follows the pathway of ionization of Mg to Mg^{2+} and the results of utilizing NaCl as an electrolyte offered more efficiency in the formation for said morphology when compared to $Na(CH_3COO)$. Therefore, the exchange of nickel for magnesium on the lattice of the structure allied with the anion chloride may be responsible for this needle-like morphology appearance.

After examining the electronic spectra (Figure 4), the data once again provide insights into the structure of the pigments. As elucidated by Qi et al. [44], the optical properties of brucite $β$-$Ni(OH)_2$ are derived from the metal d-d orbitals of nickel, considering its

octahedral configuration surrounded by six oxygens atoms. This configuration supports the Ni exchange with Mg within the structure.

The color of the pigments was characterized utilizing the CIE L*a*b*. MgO is a white powder [49], which can be attributed to magnesium lacking free electrons to excite to the 3s orbital after losing the two 3s electrons to form the Mg-O bond. However, the solid solutions synthesized showed negative a* values. In the CIE L*a*b* color space, this negative value corresponds to the intensity of green, thus confirming Ni^{2+} as the chromophore.

Regarding the biological activities of the samples, some works, such as Balaba et al. (2023) [4], indicate that MgO exhibits antimicrobial activity at a concentration of 400 µg/mL against *Staphylococcus aureus*, *Escherichia coli*, and *Candida albicans*. In contrast, our investigation highlights the Ni(Chlo) sample, which displayed inhibition at a notably lower concentration of 0.312 µg/µL, showcasing superior bacteriostatic action, particularly against Gram-negative bacteria. This outcome is noteworthy as inhibiting Gram-negative bacteria is generally considered more challenging.

Studies such as Murtaza et al. (2023) [50] and Liao et al. (2023) [51] show that MgO has better efficiency when combined with other compounds and still has a wide range of applications, such as an alternative therapeutic approach or for the treatment of plants with bacterial infections. In the work of Nguyen et al. (2018) [52] on the study of the activity of the MgO compost, the inhibition activity was 1.0 mg/mL for *Escherichia coli*, 0.7 mg/mL for *Staphylococcus aureus*, and 1.2 mg/mL for *Candida albicans*. Upon comparing these values with the data acquired in our study, it becomes evident that the MIC values were lower. Consequently, there is no necessity for such elevated concentrations to impede microbial growth, particularly when considering the impact of Ni^{2+} doping and the compound's anion on microbial inhibition activity, thereby enhancing cytotoxic effectiveness. Notably, in the case of $Ni(OH)_2$ nanoparticles, the inhibition is reportedly at 5 mg/mL, as demonstrated in the study by Chaudhari et al. (2022) [53].

5. Conclusions

A straightforward method was developed to obtain the solid solution of $[Ni_xMg_{1-x}(OH)_2]$. These solid solutions $[Ni_xMg_{1-x}(OH)_2]$ of nickel and magnesium are the result of wastewater treatment with MgO for transition metals. Therefore, discovering novel applications for these materials is an eco-friendly opportunity. This work proposed an antimicrobial inorganic pigment.

Hence, the influence of various nickel salt anions on pigment characteristics was investigated, revealing significant effects on crystalline lattice and morphology. The substitution of Mg^{2+} with Ni^{2+} in the brucite structure resulted in a lower degree of crystallinity compared to MgO_{st}. Nitrate displayed a brucite-like structure, while acetate and chloride precursors induced an interstratification disorder in the brucite phase.

Although morphology was minimally affected, chloride precursors exhibited needle-like morphology in addition to the plate-like morphology observed in all pigments. Stability tests in paint demonstrated consistent behavior in absorbance and reflectance between powder and paint interactions.

Colorimetric analysis highlighted pigment accuracy, with only chloride in paper and nitrate in plaster block showing the lower ΔE values. The antimicrobial tests revealed that all the pigments exhibit antimicrobial properties, having a biocidal effect on the Gram (+) strain *S. aureus*, or a biostatic effect on the Gram (−) strain *S. gallinarum*, at a concentration of 0.625 µg/µL in both cases. The pigments synthesized with chloride nickel salt showed a low inhibition concentration (0.312 µg/µL) for the Gram (−) strain *E. coli*, with a biostatic effect. Remarkably, the nitrate precursor salt pigment was effective against the four microorganisms that were tested.

Author Contributions: Conceptualization, C.S. and N.B.; methodology, C.S. and N.B.; validation, C.S., N.B. and A.B.S.; formal analysis, C.S., N.B. and A.B.S.; investigation, W.D.S., C.S. and A.B.S.; resources, F.J.A.; writing—original draft preparation, C.S., P.A. and A.B.S.; writing—review and editing, F.J.A. and

References

1. Pilarska, A.A.; Klapiszewski, Ł.; Jesionowski, T. Recent Development in the Synthesis, Modification and Application of $Mg(OH)_2$ and MgO: A Review. *Powder Technol.* **2017**, *319*, 373–407. [CrossRef]
2. Ansari, A.; Ali, A.; Asif, M.; Shamsuzzaman, S. Microwave-Assisted MgO NP Catalyzed One-Pot Multicomponent Synthesis of Polysubstituted Steroidal Pyridines. *New J. Chem.* **2018**, *42*, 184–197. [CrossRef]
3. Yin, J.; Zhou, G.; Gao, X.; Chen, J.; Zhang, L.; Xu, J.; Zhao, P.; Gao, F. α- and β-Phase Ni-Mg Hydroxide for High Performance Hybrid Supercapacitors. *Nanomaterials* **2019**, *9*, 1686. [CrossRef] [PubMed]
4. Balaba, N.; Jaerger, S.; Horsth, D.F.L.; Primo, J.d.O.; Correa, J.d.S.; Bittencourt, C.; Zanette, C.M.; Anaissi, F.J. Polysaccharides as Green Fuels for the Synthesis of MgO: Characterization and Evaluation of Antimicrobial Activities. *Molecules* **2023**, *28*, 142. [CrossRef]
5. Tang, Z.-X.; Lv, B.-F. MgO Nanoparticles as Antibacterial Agent: Preparation and Activity. *Braz. J. Chem. Eng.* **2014**, *31*, 591–601. [CrossRef]
6. Ohira, T.; Yamamoto, O. Correlation between Antibacterial Activity and Crystallite Size on Ceramics. *Chem. Eng. Sci.* **2012**, *68*, 355–361. [CrossRef]
7. Zhang, S.; Cheng, F.; Tao, Z.; Gao, F.; Chen, J. Removal of Nickel Ions from Wastewater by $Mg(OH)_2$/MgO Nanostructures Embedded in Al_2O_3 Membranes. *J. Alloys Compd.* **2006**, *426*, 281–285. [CrossRef]
8. Nobre, J.; Ahmed, H.; Bravo, M.; Evangelista, L.; de Brito, J. Magnesia (MgO) Production and Characterization, and Its Influence on the Performance of Cementitious Materials: A Review. *Materials* **2020**, *13*, 4752. [CrossRef] [PubMed]
9. Kumari, L.; Li, W.Z.; Vannoy, C.H.; Leblanc, R.M.; Wang, D.Z. Synthesis, Characterization and Optical Properties of $Mg(OH)_2$ Micro-/Nanostructure and Its Conversion to MgO. *Ceram. Int.* **2009**, *35*, 3355–3364. [CrossRef]
10. Navarro, A.; Martínez da Matta, M.I. Application of Magnesium Oxide for Metal Removal in Mine Water Treatment. *Sustainability* **2022**, *14*, 15857. [CrossRef]
11. Dakroury, G.A.; Abo-Zahra, S.F.; Hassan, H.S. Utilization of Olive Pomace in Nano MgO Modification for Sorption of Ni(II) and Cu(II) Metal Ions from Aqueous Solutions. *Arab. J. Chem.* **2020**, *13*, 6510–6522. [CrossRef]
12. Jiang, Y.; Shen, Z.; Tang, C.-S.; Shi, B. Synthesis and Application of Waste-Based Layered Double Hydroxide: A Review. *Sci. Total Environ.* **2023**, *903*, 166245. [CrossRef] [PubMed]
13. Shireesha, K.; Kumar, T.R.; Rajani, T.; Chakra, C.S.; Kumari, M.M.; Divya, V.; Raghava Reddy, K. Novel NiMgOH-RGO-Based Nanostructured Hybrids for Electrochemical Energy Storage Supercapacitor Applications: Effect of Reducing Agents. *Crystals* **2021**, *11*, 1144. [CrossRef]
14. Llusar, M.; Gargori, C.; Cerro, S.; Badenes, J.A.; Monrós, G. New Ceramic Pigments for the Coloration of Ceramic Glazes. *Adv. Sci. Technol.* **2014**, *92*, 148–158.
15. Pfaff, G. The World of Inorganic Pigments. *Chem. Texts* **2022**, *8*, 15. [CrossRef]
16. Monrós, G.; Llusar, M.; García, A.; Gargori, C.; Galindo, R. Development of New Ceramic Dyes. *Adv. Sci. Technol.* **2010**, *68*, 182–193.
17. Ianoş, R.; Barvinschi, P. Characterization of $Mg_{1-x}Ni_xAl_2O_4$ Solid Solutions Prepared by Combustion Synthesis. *J. Eur. Ceram. Soc.* **2011**, *31*, 739–743. [CrossRef]
18. El Jabbar, Y.; Lakhlifi, H.; El Ouatib, R.; Er-Rakho, L.; Guillemet-Fritsch, S.; Durand, B. Preparation and Characterisation of Green Nano-Sized Ceramic Pigments with the Spinel Structure AB_2O_4 (A = Co, Ni and B = Cr, Al). *Solid State Commun.* **2021**, *334–335*, 114394. [CrossRef]
19. Zou, J.; Chen, Y.; Zhang, P. Influence of Crystallite Size on Color Properties and NIR Reflectance of TiO_2@$NiTiO_3$ Inorganic Pigments. *Ceram. Int.* **2021**, *47*, 12661–12666. [CrossRef]
20. Supreetha, R.; Bindya, S.; Deepika, P.; Vinusha, H.M.; Hema, B.P. Characterization and Biological Activities of Synthesized Citrus Pectin-MgO Nanocomposite. *Results Chem.* **2021**, *3*, 100156. [CrossRef]

21. Dabhane, H.; Ghotekar, S.; Zate, M.; Kute, S.; Jadhav, G.; Medhane, V. Green Synthesis of MgO Nanoparticles Using Aqueous Leaf Extract of Ajwain (Trachyspermum Ammi) and Evaluation of Their Catalytic and Biological Activities. *Inorg. Chem. Commun.* **2022**, *138*, 109270. [CrossRef]

22. Haritha, V.; Gowri, S.; Janarthanan, B.; Faiyazuddin, M.; Karthikeyan, C.; Sharmila, S. Biogenic Synthesis of Nickel Oxide Nanoparticles Using Averrhoa Bilimbi and Investigation of Its Antibacterial, Antidiabetic and Cytotoxic Properties. *Inorg. Chem. Commun.* **2022**, *144*, 109930. [CrossRef]

23. Shah, A.; Tauseef, I.; Arfat Yameen, M.; Ben Ali, M.; Haq, S.; Elmnasri, K.; AL-Harbi, M.S.; Kashif Haleem, S.; Hedfi, A.; Ben-Attia, M. Histopathological and Hematological Investigations of Mice Model Inoculated with Nickel Oxide Nanoparticles and Bacterial Pathogens: In-Vitro and in-Vivo Antibacterial Studies. *J. King Saud Univ. Sci.* **2023**, *35*, 102456. [CrossRef]

24. WHO. E. coli. Available online: https://www.who.int/news-room/fact-sheets/detail/e-coli (accessed on 24 April 2024).

25. WHO. *WHO Fungal Priority Pathogens List to Guide Research, Development and Public Health Action*; WHO: Geneva, Switzerland, 2022; ISBN 978-92-4-006024-1.

26. WHO Global Antimicrobial Resistance and Use Surveillance System (GLASS) Report: 2022. Available online: https://www.who.int/publications/i/item/9789240062702 (accessed on 24 April 2024).

27. Rocha, M.L.M.; Balaba, N.; Jaerger, S.; Primo, J.O.; Horsth, D.F.L.; Appelt, P.; Meneguzzi, D.; Cunha, M.A.A.; Anaissi, F.J. Raw Smectite from the Guarapuava–Parana–Brasil Saturated with Copper Ions and Its Properties. *Minerals* **2023**, *13*, 785. [CrossRef]

28. Bible, B.B.; Singha, S. Canopy Position Influences CIELAB Coordinates of Peach Color. *Hortscience* **1993**, *28*, 992–993. [CrossRef]

29. Clinical and Laboratory Standards Institute (CLSI). *Reference Method for Broth Dilution Antifungal Susceptibility Testing of Yeasts*, 3rd ed.; Clinical and Laboratory Standards Institute (CLSI): Wayne, PA, USA, 2008; ISBN 1-56238-666-2.

30. Clinical and Laboratory Standards Institute (CLSI). *Methods for Dilution Antimicrobial Susceptibility Tests for Bacteria That Grow Aerobically*, 6th ed.; NCCLS document M7-A6, Suite 1400; Clinical and Laboratory Standards Institute (CLSI): Wayne, PA, USA, 2003; ISBN 610.688.0700.

31. Haynes, W.M.; Lide, D.R.; Bruno, T.L. *CRC Handbook of Chemistry and Physics*, 95th ed.; (Section 4); Taylor & Francis Group: Abingdon, UK, 2014; ISBN 978-1-4822-0868-9.

32. Vinokurov, S.E.; Kulikova, S.A.; Krupskaya, V.V.; Tyupina, E.A. Effect of Characteristics of Magnesium Oxide Powder on Composition and Strength of Magnesium Potassium Phosphate Compound for Solidifying Radioactive Waste. *Russ. J. Appl. Chem.* **2019**, *92*, 490–497. [CrossRef]

33. Yousefi, S.; Ghasemi, B.; Nikolova, M.P. Opto-Structural Characterization of Mg(OH)$_2$ and MgO Nanostructures Synthesized through a Template-Free Sonochemical Method. *Appl. Phys. A* **2021**, *127*, 549. [CrossRef]

34. Kovalenko, V.; Kotok, V. Synthesis of Nickel Hydroxide in the Presence of Acetate Ion as a «soft» Ligand for Application in Chemical Power Sources. *East.-Eur. J. Enterp. Technol.* **2019**, *6*, 6–12. [CrossRef]

35. de Oliveira, E.F.; Hase, Y. Infrared Study of Magnesium–Nickel Hydroxide Solid Solutions. *Vib. Spectrosc.* **2003**, *31*, 19–24. [CrossRef]

36. Yousefi, S.; Ghasemi, B.; Tajally, M.; Asghari, A. Optical Properties of MgO and Mg(OH)$_2$ Nanostructures Synthesized by a Chemical Precipitation Method Using Impure Brine. *J. Alloys Compd.* **2017**, *711*, 521–529. [CrossRef]

37. Yu, J.C.; Xu, A.; Zhang, L.; Song, R.; Wu, L. Synthesis and Characterization of Porous Magnesium Hydroxide and Oxide Nanoplates. *J. Phys. Chem. B* **2004**, *108*, 64–70. [CrossRef]

38. Hao, L.; Zhu, C.; Mo, X.; Jiang, W.; Hu, Y.; Zhu, Y.; Chen, Z. Preparation and Characterization of Mg(OH)$_2$ Nanorods by Liquid–Solid Arc Discharge Technique. *Inorg. Chem. Commun.* **2003**, *6*, 229–232. [CrossRef]

39. Ismail, M.; Jobara, A.; Bekouche, H.; Abd Allateef, M.; Ben Aissa, M.A.; Modwi, A. Impact of Cu Ions Removal onto MgO Nanostructures: Adsorption Capacity and Mechanism. *J. Mater. Sci. Mater. Electron.* **2022**, *33*, 12500–12512. [CrossRef]

40. Sajilal, K.; Moses Ezhil Raj, A. Effect of Thickness on Physico-Chemical Properties of p-NiO (Bunsenite) Thin Films Prepared by the Chemical Spray Pyrolysis (CSP) Technique. *Optik* **2016**, *127*, 1442–1449. [CrossRef]

41. Taibi, M.; Ammar, S.; Jouini, N.; Fiévet, F.; Molinié, P.; Drillon, M. Layered Nickel Hydroxide Salts: Synthesis, Characterization and Magnetic Behaviour in Relation to the Basal Spacing. *J. Mater. Chem.* **2002**, *12*, 3238–3244. [CrossRef]

42. Hajjaji, W.; Costa, G.; Zanelli, C.; Ribeiro, M.J.; Seabra, M.P.; Dondi, M.; Labrincha, J.A. An Overview of Using Solid Wastes for Pigment Industry. *J. Eur. Ceram. Soc.* **2012**, *32*, 753–764. [CrossRef]

43. de Andrade, T.M.; Mariani, F.Q.; Nunes Júnior, C.V.; Dalpasquale, M.; Danczuk, M.; Anaissi, F.J. Compreendendo as Propriedades (Estrutural, Espectroscópica, Colorimétrica e Térmica) de Sais de Níquel. *Matéria* **2018**, *23*, e-11976. [CrossRef]

44. Qi, Y.; Qi, H.; Li, J.; Lu, C. Synthesis, Microstructures and UV–Vis Absorption Properties of β-Ni(OH)$_2$ Nanoplates and NiO Nanostructures. *J. Cryst. Growth* **2008**, *310*, 4221–4225. [CrossRef]

45. Gottardi, W.; Nagl, M. Chlorine Covers on Living Bacteria: The Initial Step in Antimicrobial Action of Active Chlorine Compounds. *J. Antimicrob. Chemother.* **2005**, *55*, 475–482. [CrossRef]

46. Brackett, R.E. Antimicrobial Effect of Chlorine on Listeria Monocytogenes. *J. Food Prot.* **1987**, *50*, 999–1004. [CrossRef]

47. Lawson, K.; Wallbridge, S.P.; Catling, A.E.; Kirk, C.A.; Dann, S.E. Determination of Layered Nickel Hydroxide Phases in Materials Disordered by Stacking Faults and Interstratification. *J. Mater. Chem. A* **2023**, *11*, 789–799. [CrossRef]

48. Hall, D.S.; Lockwood, D.J.; Bock, C.; MacDougall, B.R. Nickel Hydroxides and Related Materials: A Review of Their Structures, Synthesis and Properties. *Proc. R. Soc. A Math. Phys. Eng. Sci.* **2015**, *471*, 20140792. [CrossRef] [PubMed]

49. Kurt, H.I.; Ergul, E.; Yilmaz, N.F.; Oduncuoglu, M. Surface Functionalization of Nano MgO Particles with Nickel and Cobalt. *Mater. Res. Express* **2019**, *6*, 0850f1. [CrossRef]

50. Murtaza, M.; Aqib, A.I.; Khan, S.R.; Muneer, A.; Ali, M.M.; Waseem, A.; Zaheer, T.; Al-Keridis, L.A.; Alshammari, N.; Saeed, M. Sodium Alginate-Based MgO Nanoparticles Coupled Antibiotics as Safe and Effective Antimicrobial Candidates against Staphylococcus Aureus of Houbara Bustard Birds. *Biomedicines* **2023**, *11*, 1959. [CrossRef] [PubMed]

51. Liao, Y.-Y.; Pereira, J.; Huang, Z.; Fan, Q.; Santra, S.; White, J.C.; De La Torre-Roche, R.; Da Silva, S.; Vallad, G.E.; Freeman, J.H.; et al. Potential of Novel Magnesium Nanomaterials to Manage Bacterial Spot Disease of Tomato in Greenhouse and Field Conditions. *Plants* **2023**, *12*, 1832. [CrossRef] [PubMed]

52. Nguyen, N.-Y.T.; Grelling, N.; Wetteland, C.L.; Rosario, R.; Liu, H. Antimicrobial Activities and Mechanisms of Magnesium Oxide Nanoparticles (NMgO) against Pathogenic Bacteria, Yeasts, and Biofilms. *Sci. Rep.* **2018**, *8*, 16260. [CrossRef]

53. Chaudhari, V.P.; Rajput, K.; Mondal Roy, S.; Chaudhuri, T.K.; Roy, D.R. Experimental and First-Principles Investigation on the Structural, Electronic and Antimicrobial Properties of Nickel Hydroxide Nanoparticles. *J. Phys. Chem. Solids* **2022**, *160*, 110367. [CrossRef]